R. & M. No. 3595

R. & M. No. 3595

MINISTRY OF TECHNOLOGY

AERONAUTICAL RESEARCH COUNCIL
REPORTS AND MEMORANDA

The Structure and Behaviour of Laminar Separation Bubbles

By M. Gaster
Aerodynamics Division N.P.L.

LONDON: HER MAJESTY'S STATIONERY OFFICE
1969
PRICE 15s. 0d. NET

The Structure and Behaviour of Separation Bubbles

By M. Gaster

Aerodynamics Division N.P.L.

Reports and Memoranda No. 3595*
March, 1967

Summary.

A study has been made of laminar separation bubbles formed over a wide range of Reynolds numbers and in a variety of pressure distributions. The structure of the bubble depended on the value of the Reynolds number of the separating boundary layer and a parameter based on the pressure rise over the region occupied by the bubble. Conditions for the bursting of 'short' bubbles were determined by a unique relationship between these two parameters. Hot-wire measurements of both mean and fluctuating velocity in the separated region, together with oscilloscope records of the fluctuations, explain some of the flow mechanisms involved.

CONTENTS

Section

* Replaces NPL Aero. Report 1181 (Revised)—A.R.C. 28 226.
(Work carried out at Queen Mary College, London University.)

1. *Introduction.*

The laminar boundary layer over the nose of a thin aerofoil at high incidence fails to remain attached to the upper surface in the region of high adverse pressure gradient that occurs just downstream of the suction peak. The separated shear layer which is formed may curve back to the aerofoil surface to form a shallow region of reverse flow known as a separation bubble. The fluid is static in the forward region of the bubble and a constant pressure region results. At high Reynolds numbers the extent of such a bubble is exceedingly small, of the order of 1 per cent chord, and the slight step in the pressure distribution produced by the dead air region has a negligible effect on the forces acting on the aerofoil. However, with a change in incidence or speed (usually an increase of incidence or a reduction in speed) the shear layer may fail to reattach and the 'short' bubble may 'burst' to form either a 'long' bubble, or an unattached free shear layer. This change in mode of reattachment can occur gradually or quite sharply, depending on the type of aerofoil. The pressure-distribution association with a long bubble is quite different from that of inviscid flow, and the forces acting on the aerofoil are therefore modified, sometimes quite drastically, by the change in mode of reattachment. In particular, bubble bursting creates an increase in drag and an undesirable change in pitching moment. If a very large bubble is formed on bursting, or if the shear layer fails to reattach, there is also an appreciable fall in lift. This is one type of stall the thin aerofoil nose stall.

The experiments discussed in this Report were carried out with the object of finding some criteria for predicting which form of bubble is most likely to arise in any given circumstances.

2. *Previous Work.*

Apart from the observations of Sir Melvill Jones[4] some 25 years ago, little work was carried out on the bubble problem until fresh interest was aroused through the use of thin aerofoil sections for reducing the effects of compressibility. As a comprehensive survey of these early experiments has already been made by McGregor[5], it is not proposed to give a detailed account here.

Von Doenhoff[2] suggested a criterion for bubble bursting which worked in some cases. He assumed that the boundary layer separates along a tangential path, that transition to turbulence takes place at a constant Reynolds number based on the distance from separation and that the turbulent layer spreads out at a fixed wedge angle. He used simple geometrical arguments to find if there was a reattachment point on the aerofoil. However, this method of predicting bubble bursting was found to apply in only a few cases and in general the method failed.

McGregor investigated the leading-edge bubbles on a sharp nosed Piercy section and a blunt thick profile having a semi-circular leading edge. He used hot-wire probes to measure mean and turbulent velocities inside the short bubbles on both aerofoils for a range of incidences and wind speeds. Although McGregor suggested a bursting mechanism he was unable to obtain sufficient data to prove his hypothesis. He argued that the supply of kinetic energy from the shear layer to the bubble must balance the loss through viscous dissipation and that it may be necessary for the bubble to expand in order to maintain equilibrium.

Owen and Klanfer[6] analysed some pressure distributions on NACA 63-009 and 64-006 aerofoils which were available for a range of incidences and Reynolds numbers. It was found that the bubbles were either 'long', $1/\delta_s^* \sim 0(10^4)$, or 'short', $1/\delta_s^* \sim 0(10^2)$, depending on whether the separation boundary layer Reynolds number $R_{\delta_s^*}$, was less or greater than about 450. The displacement thicknesses δ_s^*, were calculated from the pressure distributions. However, as all the long bubbles were formed on NACA 64-006 and all the short on 63-009, it was thought that possibly other factors could have controlled the bubble régime.

Crabtree[1] correlated large amounts of experimental data collected from a wide variety of flows by plotting log $1/\delta_s^*$ against $R_{\delta_s^*}$. Most of this data confirmed the existence of a critical Reynolds number of about 450–500 separating the two bubble régimes. However, McGregor's data gave values of 520 for the Piercy aerofoil at 5·9° incidence, 740 and 1200 for the blunt nosed model at zero and 4·2°. Other cases showing large bursting Reynolds numbers have also arisen and Crabtree attempted to use an additional parameter, based on the pressure rise over the bubble, to explain this behaviour. He suggested that there is a maximum value of this parameter σ that a short bubble can sustain, bursting occurring either through the Reynolds number falling to 450, or σ rising to a critical value of about 0·35. There is some agreement with McGregor's work, but correlation is by no means complete.

More recently Tani[8] has published a review paper on separation bubbles. His findings are similar to those of Crabtree, although from a varied collection of data on circular cylinders, elliptic sections, as well as aerofoils, he concluded that the actual critical values of the two parameters were not constant.

Some work carried out in Australia by Wallis[9,10] on high C_L aerofoils suggested that bubble bursting was associated with turbulent separation of the reattached layer. From his data there seems little doubt that in this particular case the trouble was caused by the behaviour of the turbulent boundary layer, since it showed the usual signs of incipient separation prior to nose stalling, but the writer feels that this mechanism is not the usual cause of bubble bursting on conventional aerofoils.

3. *Design Philosophy of the Test Model*

The present experimental investigation was intended to provide more data, particularly detailed information on bubble structure, over a wide range of conditions. As bubbles on different aerofoils seemed to differ slightly, it was decided to build one model arrangement which allowed both Reynolds number and pressure distribution to be continuously varied. The model used in the present series of experiments consisted of a flat plate with a small auxiliary aerofoil mounted inverted above its surface (*see* Fig. 1). The aerofoil's circulation produced a pressure distribution on the surface of the plate similar to the suction peak around the nose of a thin aerofoil at incidence, but to a large physical scale. This produced large bubbles suitable for a detailed investigation. Movement of the small aerofoil allowed a wide choice of pressure distributions on the plate boundary layer. This arrangement enabled all experiments to be carried out on a flat surface, thus removing one of the possible parameters.

It was originally intended to extend the investigation to the swept case, and the present choice of model was influenced by this consideration. The plate-aerofoil arrangement can easily be swept and difficulties arising from tunnel constraint, which always occur on large swept wings at incidence, are almost eliminated. The circulation round the small aerofoil is roughly balanced by bound vorticity of opposite sign on the plate under the aerofoil. The downwash field induced by this 'vortex-pair' system decays much more rapidly (like $1/r^2$) than that arising from a single vortex ($1/r$). Although all the work described here is on the unswept model, a similar swept version has since been used.

3.1. *Preliminary Tests*

Before attempting to build the proposed model system some brief wind tunnel tests were made on a rough mockup. An 8 in. (20 cm) chord 15 per cent thick flat bottomed section was mounted about 2 in. (5 cm) from the surface of a thin aluminium plate of 30 in. (75 cm) chord. The pressure distributions on the plate could be varied by adjusting the incidence of the aerofoil. It was found necessary to fit a trailing-edge flap to the plate to bring the front stagnation onto the upper working surface.

The pressure distributions obtained clearly showed that a separation bubble was produced by the proposed model arrangement. The flow, which was studied with the aid of a traversing pitot, was similar in all respects to a leading-edge bubble on an aerofoil. This technique for creating separation bubbles

appeared to be ideal for research purposes apart from a tendency for the small aerofoil to stall when the configuration was set up to provide large suction peaks.

3.2. *The Final Test Model*

It was thought desirable to suppress the stalling tendency of the auxiliary aerofoil by some form of boundary-layer control. Although suction probably produces the least disturbance in the outer flow it is more complicated to arrange in a small aerofoil. A simple jet entrainment scheme was therefore used. The system chosen, which is shown in Fig. 2, has the jet efflux well clear of the bubble so that the turbulence was unlikely to induce premature transition. To aid flow visualization the aerofoil was moulded from clear Perspex sheet and reinforced with two steel spars. As the jet would move the rear stagnation round to the pressure side of the aerofoil, the trailing edge of the moulding was generously radiused to assist the flow in negotiating this change in direction more easily.

The flat plate, which was also built up from Perspex sheet on steel spars, had pressure holes spaced at $\frac{1}{2}$ in. (1·25 cm) intervals along the centreline and two rows at 1 in. (2·5 cm) spacing, 12 in. (30 cm) on either side of the centre.

Details of the construction of the aerofoil and plate are given in the Appendix together with a description of the traversing gear and instrumentation.

4. *The Two-Parameter Bursting Criterion*

The laminar boundary layer on the surface of the flat plate will first be accelerated up to the peak suction and then retarded by the adverse pressure gradient. If the adverse pressure gradient is sufficient, the boundary layer will separate. Provided the free stream turbulence is low and the Reynolds number of the boundary layer at separation is less than about 1000, the flow will be laminar at separation. As laminar separation profiles are almost independent of the previous history of the boundary layer, the downstream behaviour of the flow can only depend on the local Reynolds number and pressure distribution. The fluid is practically static under the separated laminar layer so that the pressure gradient on the surface is almost zero. The shape of the dividing streamline is in fact determined by this pressure condition—the perturbation of the potential flow must be such that a constant pressure region arises under the laminar shear layer. The shape of the bubble is, therefore, dependent on the pressure distribution that would arise without separation, and the proper pressure gradient parameter to describe bubble behaviour must be based on the unseparated potential flow. A suitable non-dimensional parameter describing the pressure distribution in the region of the bubble is $(\theta_s^2/\nu)(\Delta U/\Delta x)$, where ΔU is the rise in velocity over the length of the bubble Δx. If the bubbles are long compared with the width of the suction peak, a single distribution parameter based on a mean velocity gradient may be insufficient and higher order terms will also have to be used.

Since the momentum thickness varies only slowly near separation (skin friction is small), it is a better length parameter than the rapidly changing displacement thickness used by Owen, Crabtree and others. It is also a more suitable choice as most one-parameter methods of calculating boundary layers give the value of the momentum thickness at separation. In this paper θ_s will be used as a length scale in place of δ_s^*.

If the two parameters R_{θ_s} and $(\theta_s^2/\nu)(\Delta U/\Delta x)$ do in fact control bubble behaviour, bursting should yield a unique relationship between them. To test this hypothesis the necessary quantities were measured for a number of short bubbles prior to bursting. Different flows were produced by moving the position of the suction peak along the plate: the magnitude of the peak was also varied by altering the blower power, the aerofoil incidence and height from the plate. The 'inviscid' pressure distribution (unseparated flow) was found by tripping the laminar boundary layer to a turbulent one which remained attached. It was also necessary to know the momentum thickness at separation, and this was obtained from hot-wire traverse through the boundary layer. Fig. 3 shows the data for seven bubbles on the test model, together with points calculated from McGregor's and Crabtree's work. This plot shows quite clearly that critical bursting Reynolds numbers correlate with the proposed new pressure-gradient parameter. It is worth noting that on aerofoils with small nose radii the suction peak is sharp, and as bubbles are generally quite short compared with the linear region of the adverse gradient, $\Delta U/\Delta x$ will be almost equal to dU/dx at separation. It can be shown that separation occurs when $(\theta_s^2/\nu)(dU/dx) = -0{\cdot}09$ for

this type of pressure distribution and thus for sharp nosed conventional aerofoils we can expect the critical Reynolds number for bursting to be at about 125 ($R_{\delta_3^*} = 460$). Owen's criterion applies to such aerofoils and is a special case of a more general two-parameter criterion.

5. *The Structure of the Mean Flow.*

To obtain more data on the bubble structure, hot-wire traverses and surface pressure distributions were obtained for two geometrical settings of the aerofoil (Series I and II). Measurements were made for each configuration over a sufficient range of speeds for the bubbles to pass from the highest Reynolds number short regime, through the critical bursting phase to the long bubble mode.

Results from the hot-wire are shown plotted as contours of constant velocity (as measured by the hot-wire) over the bubble. This type of plot certainly gives some idea of the flow structure, but the actual shapes of the velocity profiles also contribute and these will be shown in some cases. Some care is necessary when interpreting this data as the hot-wire device is insensitive to flow direction and it cannot, therefore, discriminate between forward and reversed flows. The non-linearity of the instrument also leads to measurements of the mean flow magnitude which are too large in the region of the reverse flow vortex where turbulence is high and the mean flow small.

5.1. *Series I Tests*

The pressure distributions for seven speeds are shown in Fig. 4. Each graph shows the actual measured pressure distribution with the bubble present, together with that obtained when the bubble was suppressed by tripping the boundary layer on the plate. As the tunnel speed was reduced the constant pressure step became progressively longer and the suction peak smaller. At the lowest speed (run (vii)), the bubble appears to exist in the 'long' mode—the pressure distribution shows a slower and smoother recovery to the unseparated curve, this being characteristic of long bubbles. However, in this particular example the bubble expansion process was gradual and there was no sharp clearcut 'burst'.

The contours of constant velocity (Fig. 5) show the general shape of the bubble: the smooth non-expanding separated shear flow, the shallow triangular dead air region and the area of turbulent mixing which causes the flow finally to reattach. As the speed is progressively reduced, the initial portion of the bubble composed of the laminar shear layer and the dead air region remains similar, even when the bubble passes into the long regime. Changes occur mainly in the turbulent mixing region which extends over an increasingly larger proportion of the bubble as the speed falls. Note that the vertical scale on these graphs has been stretched by a factor of 10 and in fact the bubbles are much shallower than might at first be thought. After separation the width of the shear layer spreads quite slowly, presumably because the stresses are all viscous and thus small. But, at the end of the dead air region, transition to turbulence considerably accelerates the expansion process, smoothing out the velocity profiles. Also at the end of the dead air region the profiles show a sudden increase in the magnitude of the velocity close to the wall. This apparent wall shear stress usually has a minimum before increasing again to the fully turbulent value. Although the actual mean shear stress must be zero at reattachment the unsteady nature of the flow and the non-linear characteristics of the hot-wire can only indicate a minimum value. This point was found to coincide reasonably well with the reattachment position obtained by tufts and surface indicators, and for most of the work reported here the reattachment point was determined in this way from the contour plots.

5.2. *Series II Tests*

The data obtained for the second model configuration shown in Figs. 6, 7 and 8 is very similar to that of the first, except that in this case the bubbles formed at the lowest tunnel speeds were definitely in the long state. The contours of constant velocity for these long bubbles are similar to those of the shorter type in the initial laminar region, but only slowly develop into a fully attached layer after transition—the mixing process appears to cover a greater distance before achieving attachment.

5.3. *Bubble Length*

Fig. 9i shows the ratio of bubble length to separation momentum thickness plotted against Reynolds number for all the bubbles arising in the two series of tests. At high values of R_{θ_s} the curves are smooth

and show the expected steady decrease in length with increase in Reynolds number, while at low values considerable scatter is evident, particularly for points arising from long bubbles. A more consistent trend is given by the ratio of the length of the dead air region to momentum thicknesses as shown in Fig. 9ii. Again at low values of R_{θ_s} one or two points lie off the general trend which shows that λ/θ_s varies only slowly with R_{θ_s}.

6. *Turbulence Measurements*

Having investigated the mean flow structure of both long and short bubbles it was thought desirable to make a brief survey of the turbulent velocities. However, to carry out such an investigation properly required rather more time than was available. Nevertheless, some information, mainly of a qualitative nature, was obtained using relatively simple instrumentation. All the measurements discussed in this Report were made with a thick (0·001 in. (25 μm) dia.) nickel wire feeding an uncompensated a.c. coupled amplifier. This combination had a serious loss in sensitivity at both high and very low frequencies, but as most of the interesting part of the signal falls in the central portion of the spectrum one can expect the measurements to be reasonably helpful. As the turbulent fluctuations were large the simple perturbation hot-wire theory cannot apply. The flow structure is so complicated in the mixing region, where even the mean velocities are unknown, that valid corrections are impossible to apply. The results presented here have been left uncorrected, leading to large measurement errors in certain regions of the bubble. Nevertheless, some useful information may be obtained from the data.

The root mean square (R.M.S.) values of the velocity fluctuations were measured throughout the whole region of a short bubble. The mean square of the electrical signal was obtained from a vacuo-thermo junction which fed a spot galvanometer. The maximum value of apparent turbulence (as measured by the hot-wire) was found to be about 16 per cent in the middle of the shear layer at the end of the dead air region. McGregor also measured bubble turbulence, but with better instrumentation, and he obtained a maximum level of 12 per cent. This difference is well within the accuracy of the present measurements. The map of turbulence intensity is shown plotted with the mean flow on Fig. 10.

To see how the turbulence developed as the bubble passed from a high Reynolds number short bubble to a long one, measurements were made along the centre of the shear layer ($U/U_1 = \frac{1}{2}$) for Series II bubbles. McGregor used the same technique over a limited range of velocities in short bubbles, but he chose the line $U/U_1 = \frac{1}{4}$; the midpoint of the shear layer chosen by the writer seems more appropriate since the maximum signal level appears roughly there. The measurements were taken with a filter between the hot-wire pre-amplifier and the main amplifier to accentuate the high frequency part of the signal. It is not possible directly to compare the actual levels of turbulence at different speeds, for the spectra change with speed so that strictly the filter should have been changed for each run. Therefore the strength of the signal relative to the maximum value has been plotted in Fig. 11 against the distance from separation, suitably non-dimensionalized by the separation momentum thickness. The results show the same trend of a rapid amplification followed by saturation, but the curves do not fully collapse. This is perhaps not surprising as the Reynolds number and the height of the separated flow above the boundary, which both affect the stability, differ considerably over the range of bubbles tested. There appears to be no significant difference between short and long bubbles, transition being completed in a distance of between 130 and 180 momentum thickness.

6.1. *Oscilloscope Records*

Further information of a qualitative nature can be obtained from an examination of the oscilloscope records of the hot-wire signals taken at various distances from separation along the centreline of the shear layer. Three of the bubbles in Series II were chosen for these tests; the short bubbles (ii) and (iv) and the long bubble of run (vii).

The first group of traces shown in Fig. 12 are for the short bubble (ii) at a free stream tunnel speed of 59 ft/sec. (17·7 m/sec.). Shots (a) and (b) are for stations upstream of the separation point. Nevertheless, they show a fairly high level of turbulence, mainly of a low frequency character. These signals have a high harmonic content which is almost certainly caused by the growth of instability waves in the attached boundary layer. After separation has occurred these low frequency disturbances decay, presumably

because the velocity profiles are no longer unstable to such long waves, and the higher frequency oscillation characteristic of shear layers take precedence. These high frequency components amplify rapidly and eventually become more random in character and fully turbulent.

The second set of oscilloscope records, Fig. 13, were taken in bubble (iv) at a speed of 40·9 ft/sec. (12·3 m/sec.). The low frequency signal which occurred in the previous higher Reynolds number case does not appear in this sequence, presumably because the attached boundary layer is stable at this Reynolds number. Oscillations of about 1000 c/s appear in the separated layer and these grow rapidly, although the amplitude of the signal does not appear to be very steady. Record (e), which shows occasional frequency doubling, suggests that the amplitude of the high frequency fluctuation is large enough for flow reversal.

The third group of oscillograph records, Fig. 14 are for the case of a low Reynolds number long bubble (vii). The nature of the hot-wire signal is quite different from that of the two previously discussed short bubble cases. The hot-wire output is composed of short pulses of oscillation with long gaps of fairly steady flow in between. The signal further aft shows that these patches of disturbances become more frequent and longer, also these signal pulses become more periodic—probably due to a certain amount of selective amplification. Far enough downstream at the end of the 'dead air' region these pulses have expanded to form a continuous turbulent signal. The behaviour of these oscillations in the long bubble are more clearly shown in the continuous recordings taken at film speeds of 5 in./sec (12·5 cm/sec) and at 0·5 in./sec (1·25 cm/sec) in Fig. 15. The intermittent character of the signal is revealed particularly by the slow speed recording taken at 0·5 in./sec. By coupling the bridge signal directly to one beam of the oscilloscope it was possible to observe both the high and low frequency oscillations at the same time. In Fig. 16 where these results are shown, it can be seen that there is a patch of high frequency turbulence whenever the low frequency wave reaches a maximum. This behaviour probably arises because the low frequency oscillations distort the velocity profile in such a way that its stability slowly varied with time, and conditions for the rapid amplification of high frequency waves only occur intermittently.

6.2. *Acoustically Excited Disturbances*

It was found that the strength of the high frequency periodic oscillations, which had been detected in the separated shear layer with a hot-wire, could be increased momentarily by striking the walls of the contraction. In fact, waves were so easily generated by sound that it was thought worth trying to generate them artificially so that a more detailed investigation could be made. A 12-inch (30 cm) 10-watt loudspeaker mounted on the tunnel roof was found to produce detectable oscillations in the shear layer with a quite small amount of power feeding the speaker, of the order of $\frac{1}{3}$ watt. Particularly strong signals were generated when the excitation frequency was close to that of the naturally occurring free waves.

Initial attempts to generate waves off resonance produced beating. This trouble was traced to the a.c. fan motor which also produced sufficient sound to excite waves. The tunnel could thus only be driven by a $\frac{3}{4}$ horsepower (500 watts) d.c. motor which was sufficiently silent for these particular experiments; unfortunately this limited the maximum speed of the tunnel to about 12 ft/sec (3·6 m/sec).

At any station in the bubble which gave a clear steady signal in response to the speaker it was possible to observe the relative phase of the electrical input and the hot-wire output by using the speaker input signal as a brightness modulation on the hot-wire trace. On moving the probe downstream the brightness modulation spot moved along the wave and it was seen that the disturbance was indeed a travelling wave which moved downstream at roughly half the speed of the external flow.

Using a transistorized pre-amplifier with a gain of about 15 and a tunable resistance-capacity coupled feedback amplifier as a narrow band filter, quite a clean signal could be obtained. Fig. (17) shows this signal with brightness modulation together with the direct bridge output d.c. coupled. The amplitude of the high frequency component slowly varies in sympathy with the low frequency fluctuation, but with a slight lag. The improved signal was sufficiently clearly defined to enable measurements of amplitude and phase—or rather the time average values—to be made. This was accomplished by the squaring technique used in turbulence work.

6.2.1. *Short bubble measurements.* Measurements of phase and amplitude were taken over the whole region of a short bubble, excited at 130 c/s, which was the frequency of maximum excitation. A

typical profile is shown in Fig. 18 and the contours are shown in Fig. 19. The magnitude of these forced oscillations is unknown and the numbers on the contour map are only relative. Without a knowledge of the theoretical distributions of velocity fluctuations in a shear layer near a wall it is difficult to interpret this data in detail. However, there are some significant facts that can be deduced from these measurements. The disturbance amplitude, which grows exponentially with distance, has a maximum value along the centre of the shear layer and is thus similar to the overall turbulence shown in Fig. 10. The phase of the signal, which varies with the distance from the shear layer in the outer portion of the profile, is reflected in the oblique wave-fronts shown on the contour plot. If the waves were temporally growing Tollmein-Schlichting waves such a phase shift could not be explained, for in the outer parallel mean flow the disturbance behaves like $e^{-\alpha y}$, where α is the real wave-number. However, for spatially growing modes (Gaster[3]) α is complex ($\alpha = \alpha_r + i\alpha_i$) so that one would expect an oblique wave when amplification occurs. In fact α_i, the rate of amplification, can be calculated from the slope of the phase plot. The value obtained is $-0{\cdot}40$, which compares well with $-0{\cdot}43$, the value found directly from the increase in amplitude along the shear layer. As the disturbance decays like $e^{-\alpha_r y}$ in the outer region, a simple logarithmic plot of amplitude against y, the distance from the boundary, gives α_r. From Fig. 18 α_r was found to be $1{\cdot}45$ which is quite close to $1{\cdot}32$, the value obtained directly from the wavelength on the contour plot. Since α_r could be found fairly well from measurements taken solely along one profile in the outer flow, a series of tests were made covering input frequencies from 80 to 170 c/s in order to compare experimental values with theory. These are plotted in Fig. 20 with the curve for the inviscid modes of the simple velocity profile composed of linear segments (Gaster[3]).

6.2.2. *Long bubble measurements.* It was originally intended to investigate the nature of acoustically excited waves in a long bubble shear layer to compare the behaviour with that of a short bubble, but it was not found possible to generate waves which were sufficiently steady. The long bubble (vii) of Series II was chosen for the work and the records with sound shown on Fig. 21 can be compared with the unexcited signal of Fig. 16. The response varied so much from moment to moment that meaningful measurements could not be made. These large variations in sensitivity were presumably associated with the slow oscillations of the mean flow, which are more violent in the long bubble.

7 *Conclusions*

The artificially generated disturbances in the separated laminar flow were travelling waves, which grew spatially along the shear layer. These waves were of the type described by theory for complex wave-number modes. The overall pattern of amplitude distribution was similar to that arising from natural oscillations and it is not unreasonable to conclude that most of the 'turbulence' measured in the flow prior to transition was due to instability waves. The instability of the separated layer may be strongly influenced by the height from the wall. Thus the low frequency motion of the bubble, probably a vertical oscillation of the shear layer, has some effect on the instantaneous growth of waves. Any such slow motion of the bubble as a whole will distort the shape of the velocity profile thus also altering the stability of the flow. This variation in sensitivity from moment to moment is more pronounced in long bubbles, where the low frequency motion is more violent. Conditions for the rapid growth of oscillations only arise occasionally. Nevertheless, the mean rate of growth along the shear layer seems to be roughly the same for all bubbles: the stabilizing effect of low Reynolds number in the long bubble case seems to be compensated by the greater height of the shear layer, and transition appears to be complete between 130 and 180 momentum thicknesses from separation. The end of the dead air region roughly coincides with this transition point and a plot of this length shown in Fig. 9 indicates that it is not influenced to any great extent by the Reynolds number. The structure of the flow in the forward regions of both long and short bubbles seems to be similar up to transition.

From simple dimensional arguments it was suggested that the structure of the bubble is dependent on the two parameters R_{θ_s} and $(\theta_s^2/\nu)(\Delta U/\Delta x)$. Conditions for bursting did, in fact, show a strong correlation between these quantities and one is tempted to extend this idea further. Consider a point Q on the $\bar{P} \sim R_\theta$ plane representing a short bubble well away from bursting (*see* Fig. 22). On reducing the wind-tunnel speed the value of R_{θ_s} will decrease; $\bar{P}$ may also change due to the increase in bubble length, but

it is not immediately obvious whether it increases or decreases with a reduction in free stream speed. As the speed is continually reduced it is possible to map out a trajectory on the $\bar{P} \sim R_{\theta_s}$ plane to see how the two controlling parameters behave near bursting. A slight alteration in tunnel speed changes θ_s and R_{θ_s} directly, but as the bubble length also changes and modifies the upstream pressure field a further change in both results. If this feedback cycle converges, the process is stable—a slight variation in speed results in only a small change in bubble length. However, one can imagine a situation when the process is a divergent one such that a slight reduction in speed causes the bubble to expand rapidly and burst.

The experimental data shown in Fig. 23 describes these trajectories for four different bubbles. Apart from one point the paths are fairly clearly defined, although a closer spacing of the points would help to show the behaviour in more detail. The type of burst seems to depend on the shape of these curves as they approach bursting. Two of the curves blend into the bursting criterion line and describe a smooth expansion type of burst, while the remaining pair, which approach the critical line more steeply, exhibited a violent burst. As the trajectories can cross it is clear that the path, and thus the subsequent behaviour of the bubble, is not solely a function of R_{θ_s} and $\bar{P}$. The upstream flow must affect the feedback cycle and thus have a controlling influence, but it is not at all clear what parameters are important. Clearly more data is needed before the processes involved are sufficiently clearly understood for an analytical approach.

Acknowledgement

The author wishes to acknowledge the help and advice given by Professor A. D. Young and Dr. L. G. Whitehead at Queen Mary College, London University, where the research was carried out.

LIST OF SYMBOLS

x	Distance from model leading edge in the stream direction
y	Normal distance from the surface of the model
$\Delta x, l$	Length of separated flow
λ	Length of dead air region
θ	Boundary-layer momentum thickness
δ^*	Boundary-layer displacement thickness
U	Velocity in the x direction
ΔU	Change in velocity over the region of separated flow based on the inviscid pressure distribution
P	Pressure
ρ	Mass density
ν	Kinematic viscosity
$\alpha = \alpha_r + i\alpha_i$,	The wavenumber (r and i here denote the real and imaginary parts)
$R_{\theta_s} = \frac{U_s \theta_s}{\nu}$,	The separation Reynolds number
$\bar{P} = \frac{\theta_s^2}{\nu} \frac{\Delta U}{\Delta x}$,	A pressure-gradient parameter
$C_p = \frac{P - P_\infty}{\frac{1}{2}\rho U_\infty^2}$	The pressure coefficient

$$\sigma = \frac{C_{pr} - C_{ps}}{1 - C_{ps}}$$

Subscripts

r	Reattachment
s	Separation
∞	The undisturbed stream
1	Outside the boundary layer

REFERENCES

No.	*Author(s)*	*Title, etc.*
1	L. F. Crabtree	The formation of regions of separated flow on wing surfaces. Part I. Low-speed tests on a two-dimensional unswept wing with a 10 per cent thick RAE 101 section. Part II. Laminar separation bubbles and the mechanism of the leading-edge stall. A.R.C. R. & M. 3122. 1959.
2	A. E. Von Doenhoff	A preliminary investigation of boundary-layer transition along a flat plate with adverse pressure gradient. NACA TN 639. March, 1938.
3	M. Gaster	The role of spatially growing waves in the theory of hydrodynamic stability. *Progress in Aeronautical Sciences*, Vol. 6, 1965. Pergamon Press.
4	B. M. Jones	Stalling. *J. R. Aero. Soc.*, Vol. 38, 1934. pp. 753–770.
5	I. McGregor	The regions of local boundary-layer separations and their role in the stalling of aerofoils. Ph.D. Thesis, Queen Mary College, London, 1954.
6	P. R. Owen and L. Klanfer ..	On the laminar boundary-layer separation from the leading edge of a thin aerofoil A.R.C. C.P. 220. 1953.
7	W. Schwier	Unpublished German work.
8	I. Tani	Low speed flows involving bubble separations. *Progress in Aeronautical Sciences*, Vol. 5, 1964. Pergamon Press.
9	R. A. Wallis	The turbulent boundary layer on the articulated nose of a thin wing provided with air jets. ARL/A.141, October, 1954.
10	R. A. Wallis and N. Ruglen ..	Note on the breakdown of the laminar separation bubble on the nose of a thin wing. ARL/A.161, May, 1957.

APPENDIX

A1. *The aerofoil*

The jet entrainment system chosen for reducing the stalling tendency of the auxiliary aerofoil was based on the work of Schwier[7], who tested wings with jets emanating from the lower surface for a range of jet efflux angles. He found that the maximum lift increment occurred when the jet was directed forward at 45° and this configuration was therefore chosen for the present model. The aerofoil was moulded round a 15 per cent thick flat-bottomed wooden aerofoil former from $\frac{1}{8}$ in. (3 mm) Perspex sheet. The 0·03 in. (0·75 mm) wide slot was cut with a slitting saw, short supporting sections being left every 6 in. (15 cm). The rear reinforcing spar had a series of holes drilled to enable the air supply, which was derived from a $2\frac{1}{2}$ BHP (1·8 kW) centrifugal compressor, to reach the narrow slot. The aerofoil was mounted horizontally across the 4 ft (1·2 m) working section so that the incidence could be changed from outside the tunnel by a worm gear drive.

A2. *The flat plate*

To provide an adequately stiff structure the plate was made from two Perspex sheets separated by a number of $\frac{1}{2}$ in. $\times \frac{3}{8}$ in. (1·25 cm × 1·0 cm) spars spaced at 6 in. (15 cm) intervals along the chord. Countersunk screws passing through the $\frac{1}{8}$ in. (3 mm) Perspex lower skin and through clearance holes in the steel spars were threaded into blind tapped holes in the $\frac{1}{4}$ in. (6 mm) upper plate, care being taken to ensure that these tapped holes did not break through the top surface of the upper plate. This model was fitted with over 100 pressure holes of 0·03 in. (0·75 mm) diameter, about 80 of which were stationed at $\frac{1}{2}$ in. (1·25 cm) intervals along the centre line and the remainder spaced 1 in. (2·5 cm) along lines 12 in. (30 cm) either side of the centre. These pressure tappings were connected to long lengths of 1·5 mm bore plastic tubing which were led out of the trailing edge of the plate in two bundles, one at each side of the tunnel. The 30 in. (75 cm) chord plate was fitted with an adjustable 3 in. (7·5 cm) aluminium trailing edge flap to enable the position of the front stagnation point to be forced round to the top surface. The leading edge was built up and shaped as shown in the sketch, Fig. (24), the lower surface being deliberately left with a sharp corner to fix the transition point. The plate was fitted into the tunnel on a pair of rails bolted to the tunnel walls in such a way that the plate could be adjusted to occupy any desired position relative to the fixed aerofoil.

A3. *The wind tunnel*

This investigation was carried out in the wooden 39 in. × 48 in. (1 m × 1·2 m) closed circuit low turbulence tunnel at Queen Mary College. The power was supplied by a 27 BHP (20 kW) slip ring induction motor controlled in steps by the addition of resistance to the rotor circuit. A $\frac{3}{4}$ HP (500 W) compound wound d.c. motor could be coupled to the same shaft as the main motor to provide a fine speed control between the ten fixed steps. The turbulence level was reasonably low, of order 0·05 per cent, at low speeds, but above about 60 ft/sec (18 m/sec) increased somewhat, probably due to the considerable amount of motor noise present. At very low speed when the d.c. motor alone was used, that is, at less than 12 ft/sec (3·6 m/sec), the turbulence was very probably much smaller, of order 0·02 per cent, due to the decrease in the sound level generated by the power plant.

A4. *Pressure distributions*

A standard 36-tube bank of water manometers of the inclined type was used for the measurement of the pressure distribution along the surface of the plate. At the lower range of velocities used it was necessary to set the inclination of the tubes only a few degrees from the horizontal, and the zero errors in the tubes then became significant and corrections had to be made to each reading.

A5. *Tunnel speed*

The speed of the tunnel was monitored by a Betz manometer during the high speed run; but for the lower speed experiments, where it was necessary to measure pressure heads of the order 30×10^{-4} ft (1 mm) of water, a Chattock–Frey gauge was employed. The gauge was filled with silicone fluid (MS 200/1) instead of the usual rather viscous purified paraffin oil. Since the viscosity of this silicone fluid is roughly

the same as water the gauge had a much more lively response and was therefore more easily and quickly balanced. Due to its strong water repellant properties, the silicone fluid had the added advantage that the bubble of the gauge can be reformed after it has been inadvertently 'burst'.

A6. *Traversing gear*

To carry out detailed probe measurements within the bubble it was necessary to be able to move the instrument easily from one station to another while the tunnel was running, and to know the co-ordinates of these stations to good accuracy. The required movement of the probe head was about 24 in. (0·6 m) longitudinally and $1\frac{1}{2}$ in. (3·8 cm) vertically to cover the whole of a long bubble. For the swept model some rotational motion was also provided.

The traversing apparatus is shown in Fig. 25. The main boom supporting the slide was mounted by a strut rigidly bolted to the rear of the plate and held in place by tensioned wires to the tunnel walls, providing a surprisingly stiff assembly. Both the longitudinal and vertical motions were driven by electric motors through flexible cables, the position of the probe being indicated by the readings of the counters fitted to these motors. In this way it was possible easily to read the vertical position to 0·001 in. (25 μm) and the horizontal to 0·01 in. (250 μm), with a negligible amount of backlash in the system. The rotational motion was provided by a hand wheel *via* another flexible drive cable. The cable drive motors were operated by a pair of micro-switches wired up so that forward motion occurred on pressing one key, and the motion was reversed on pressing the other. The two micro-switches controlling the motors were conveniently connected to the motor counter unit by long lengths of flex, thus allowing the operator either to sit at a desk with all the hot wire gear, or to work inside the tunnel setting up to the probe.

No fairing was built round the instrument because it was felt that the increase in cross sectional area would probably increase the interference on the plate over that caused by the bare structure.

A7. *Probe measurements*

The measurement of 'mean' velocities within the bubbles could have been carried out using either small pitot tubes or hot-wire anemometers. Pitot tubes have directional sensitivity so one can theoretically find whether the flow is in the forward or reverse direction at any point in a steady flow, but in the highly turbulent flow near the reattachment point of the bubble it is doubtful whether this property would still apply. The main disadvantage of this type of probe is that one also needs to know the value of the static pressure, which varies across the flow and is very difficult to measure.

The hot-wire is sensitive to the velocity normal to the wire and it therefore completely fails to detect the flow sense. However, this may not always be an important factor, for in most cases one can deduce the flow direction if this is required. Both the hot-wire and the pitot tube have highly non-linear characteristics and therefore they fail to give meaningful readings in a highly turbulent field superimposed on a relatively small mean flow, such as occurs in the reverse flow vortex region just above the reattachment point. It is not possible to find the true mean velocity in these regions of flow with either type of instrument; indeed, no instrument has yet been devised which is capable of giving a true mean velocity in these conditions. Nevertheless, contour plots of lines of constant apparent velocity as measured by the hot-wire do indeed reveal the general structure of the bubble, and following McGregor, this instrument was again chosen for this investigation.

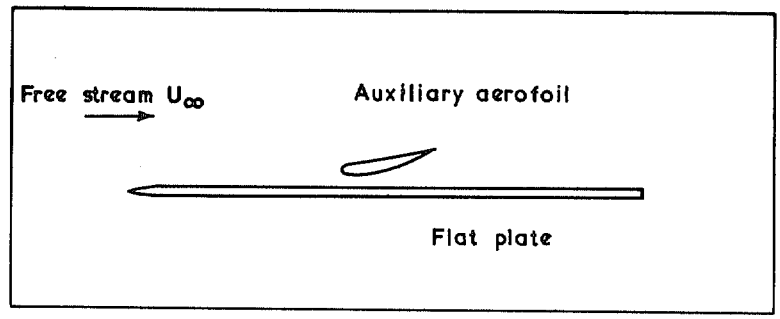

FIG. 1. Special model.

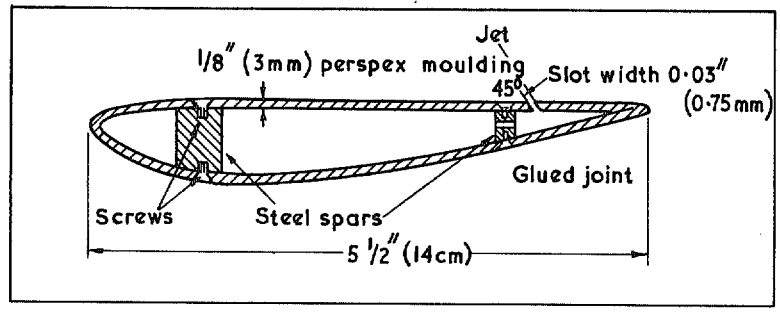

FIG. 2. Blowing aerofoil.

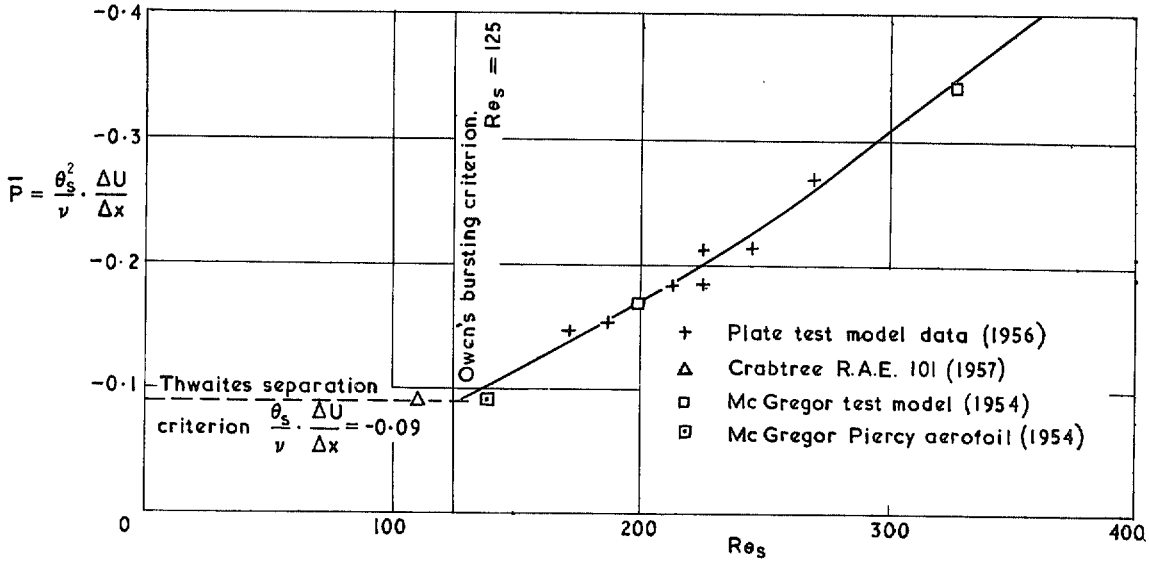

FIG. 3. Relationship between R_{θ_s} and P at bursting.

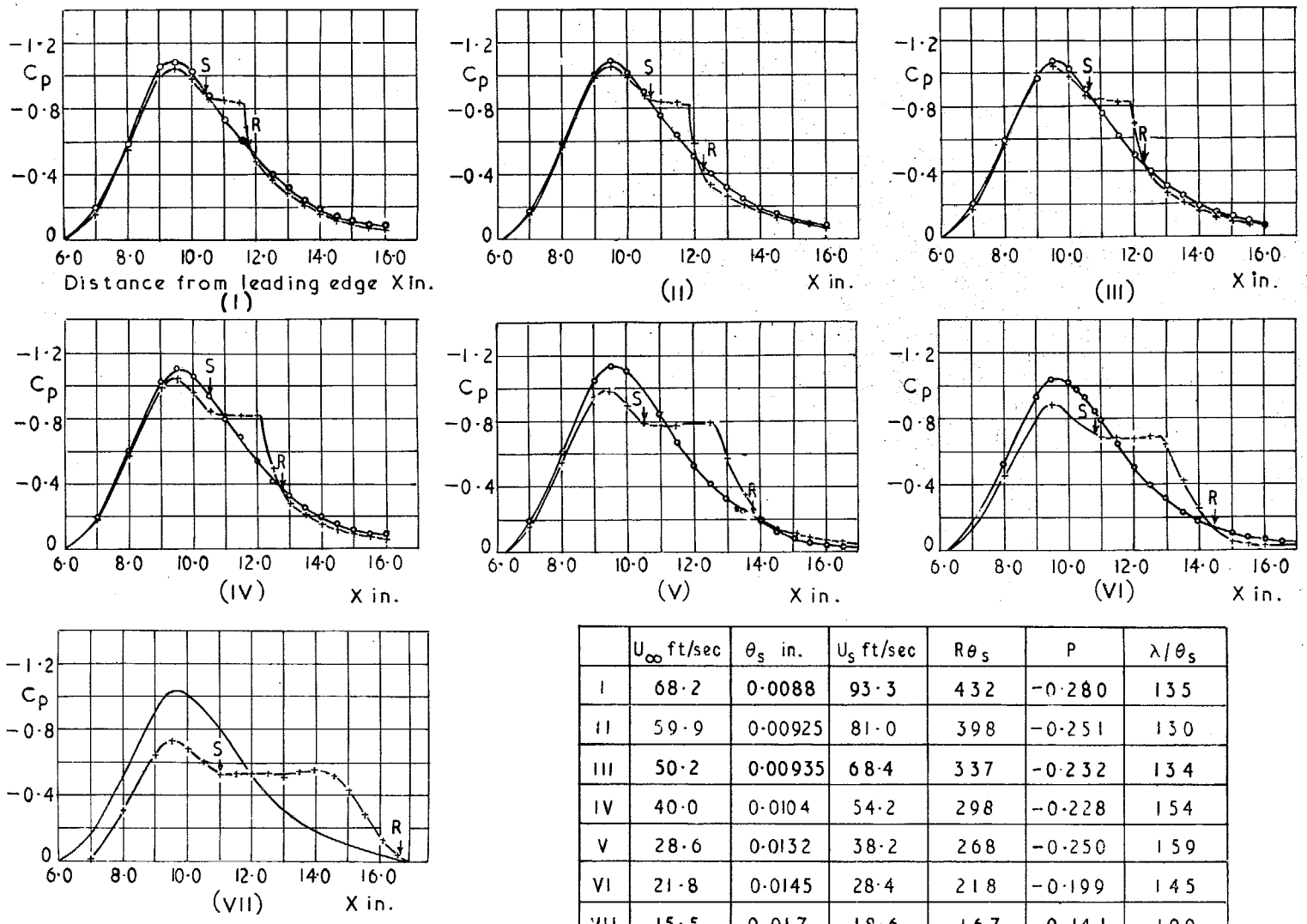

	U_∞ ft/sec	θ_s in.	U_s ft/sec	$R\theta_s$	P	λ/θ_s
I	68·2	0·0088	93·3	432	−0·280	135
II	59·9	0·00925	81·0	398	−0·251	130
III	50·2	0·00935	68·4	337	−0·232	134
IV	40·0	0·0104	54·2	298	−0·228	154
V	28·6	0·0132	38·2	268	−0·250	159
VI	21·8	0·0145	28·4	218	−0·199	145
VII	15·5	0·017	18·6	167	−0·144	190

FIG. 4. Pressure distributions. Series I.

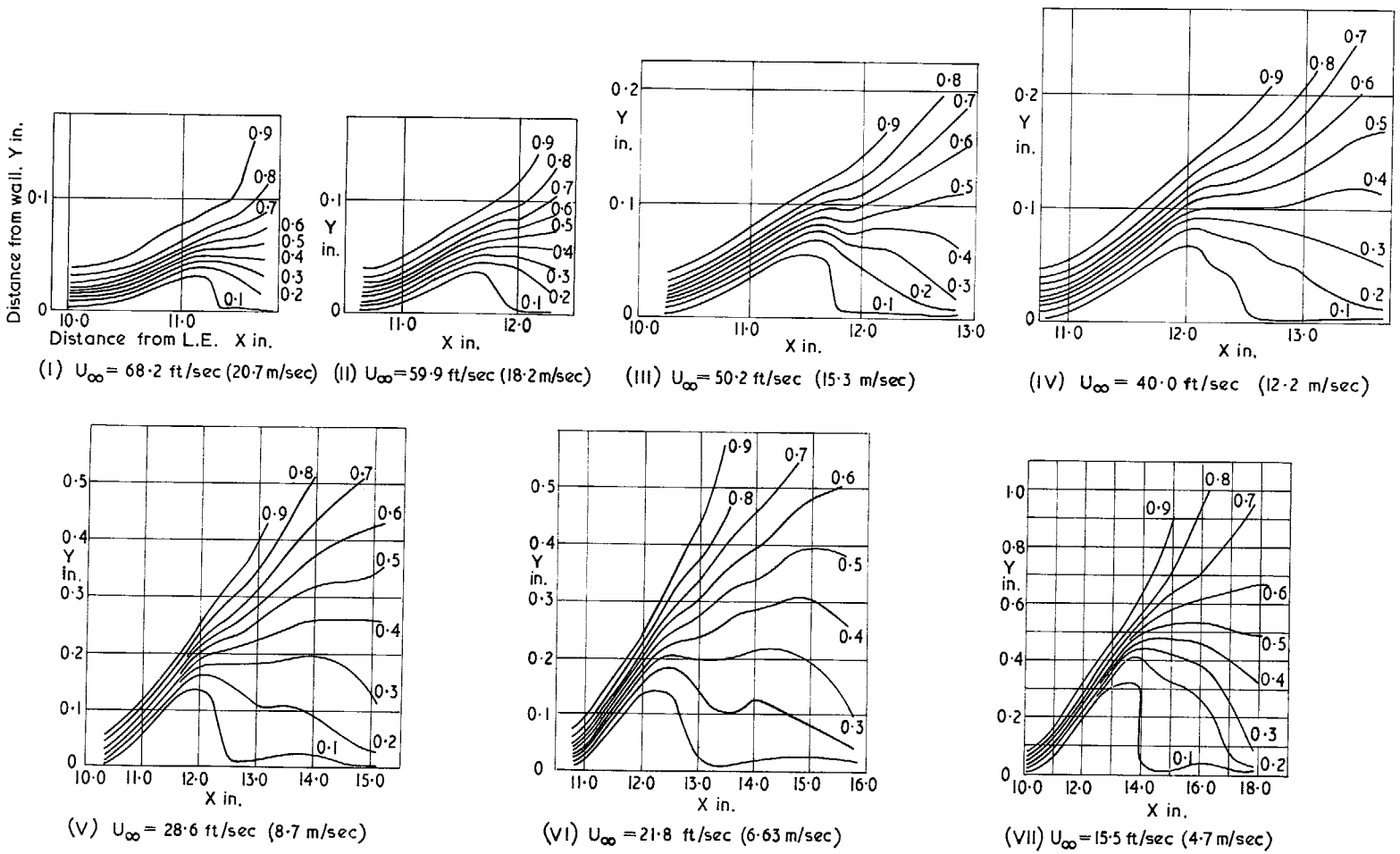

FIG. 5. Hot-wire velocity contours. Series II.

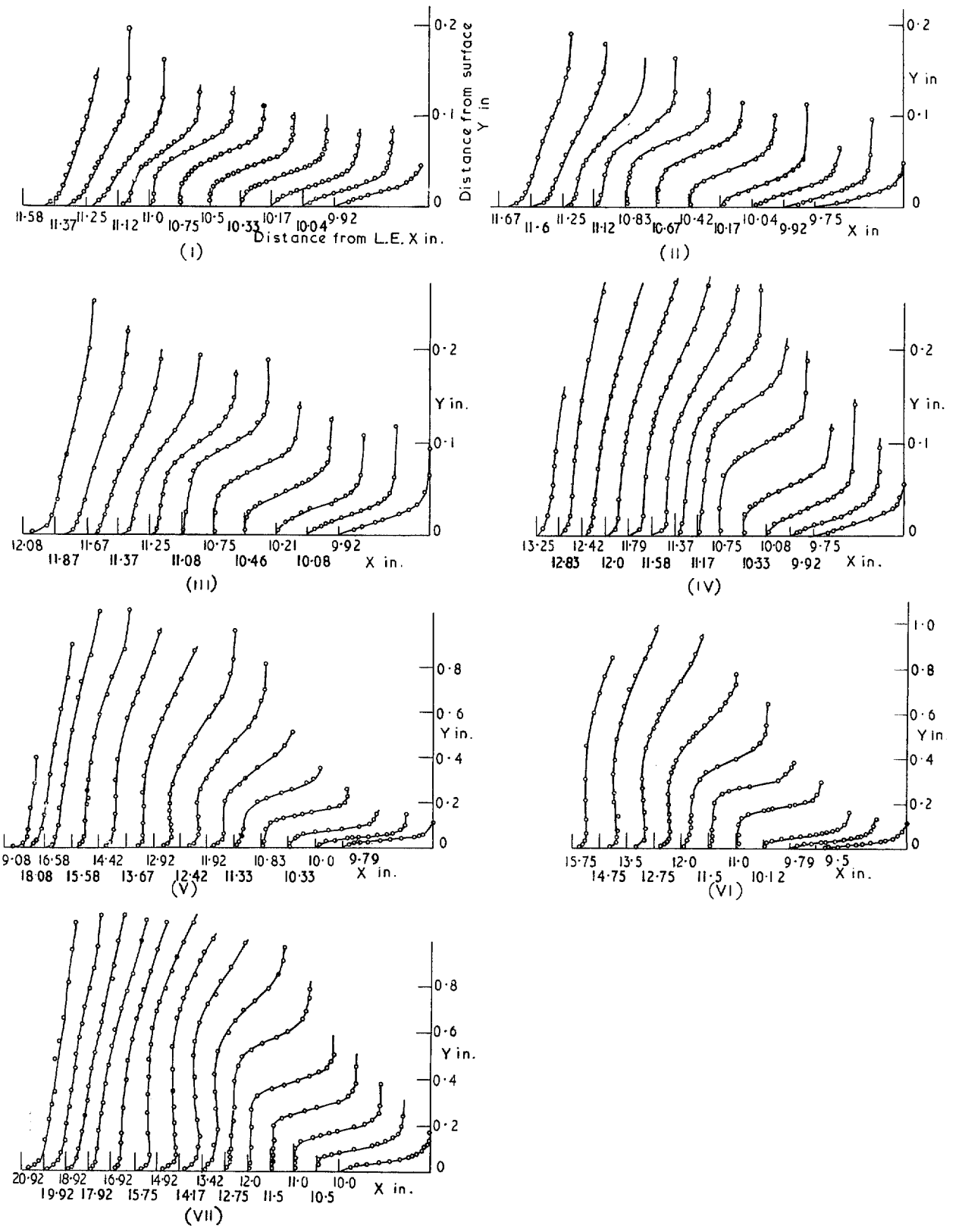

FIG. 6. Velocity profiles measured with a hot-wire. Series II.

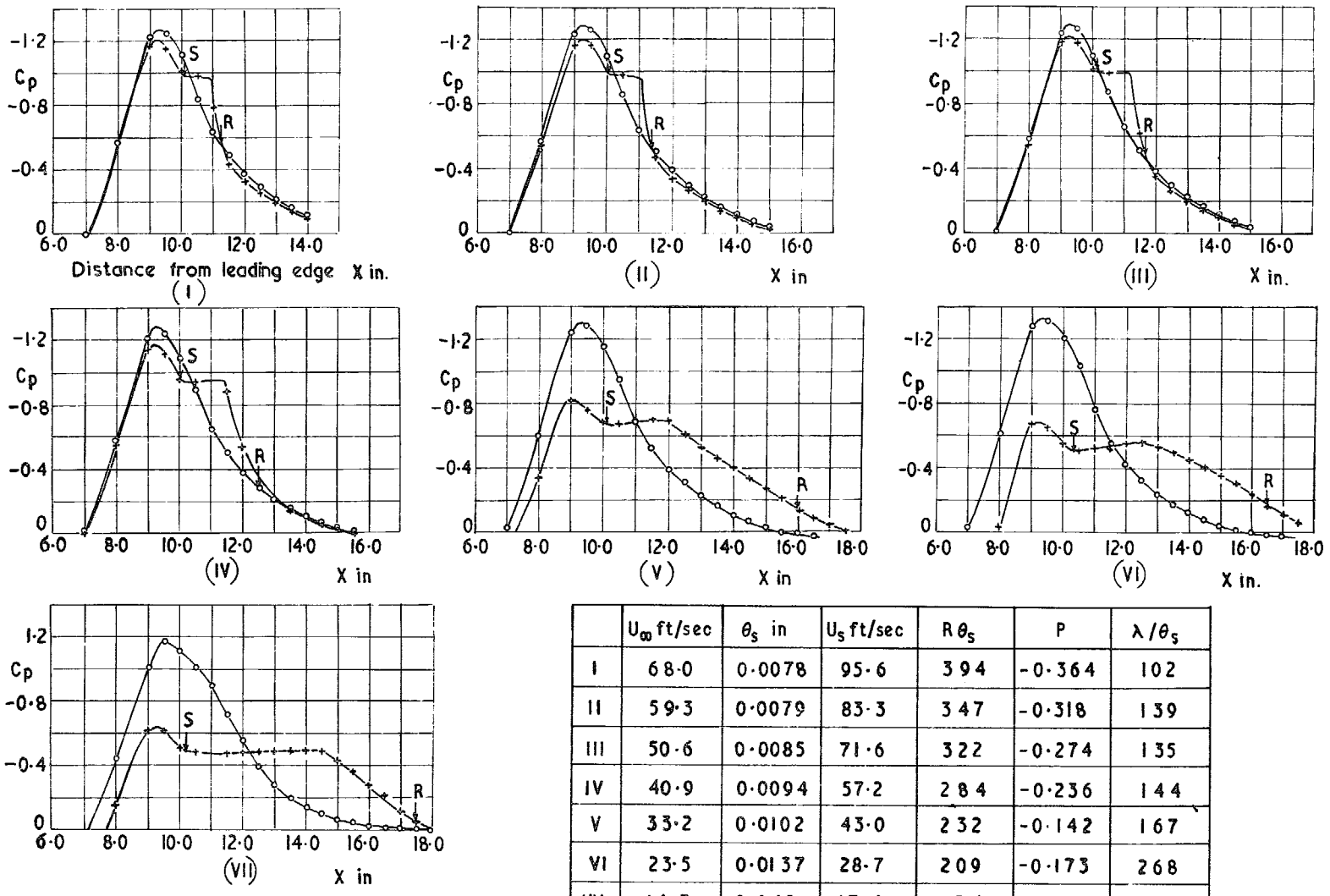

	U_∞ ft/sec	θ_s in	U_s ft/sec	$R\theta_s$	P	λ/θ_s
I	68·0	0·0078	95·6	394	-0·364	102
II	59·3	0·0079	83·3	347	-0·318	139
III	50·6	0·0085	71·6	322	-0·274	135
IV	40·9	0·0094	57·2	284	-0·236	144
V	33·2	0·0102	43·0	232	-0·142	167
VI	23·5	0·0137	28·7	209	-0·173	268
VII	14·3	0·048	17·6	136	-0·094	297

FIG. 7. Pressure distributions. Series II.

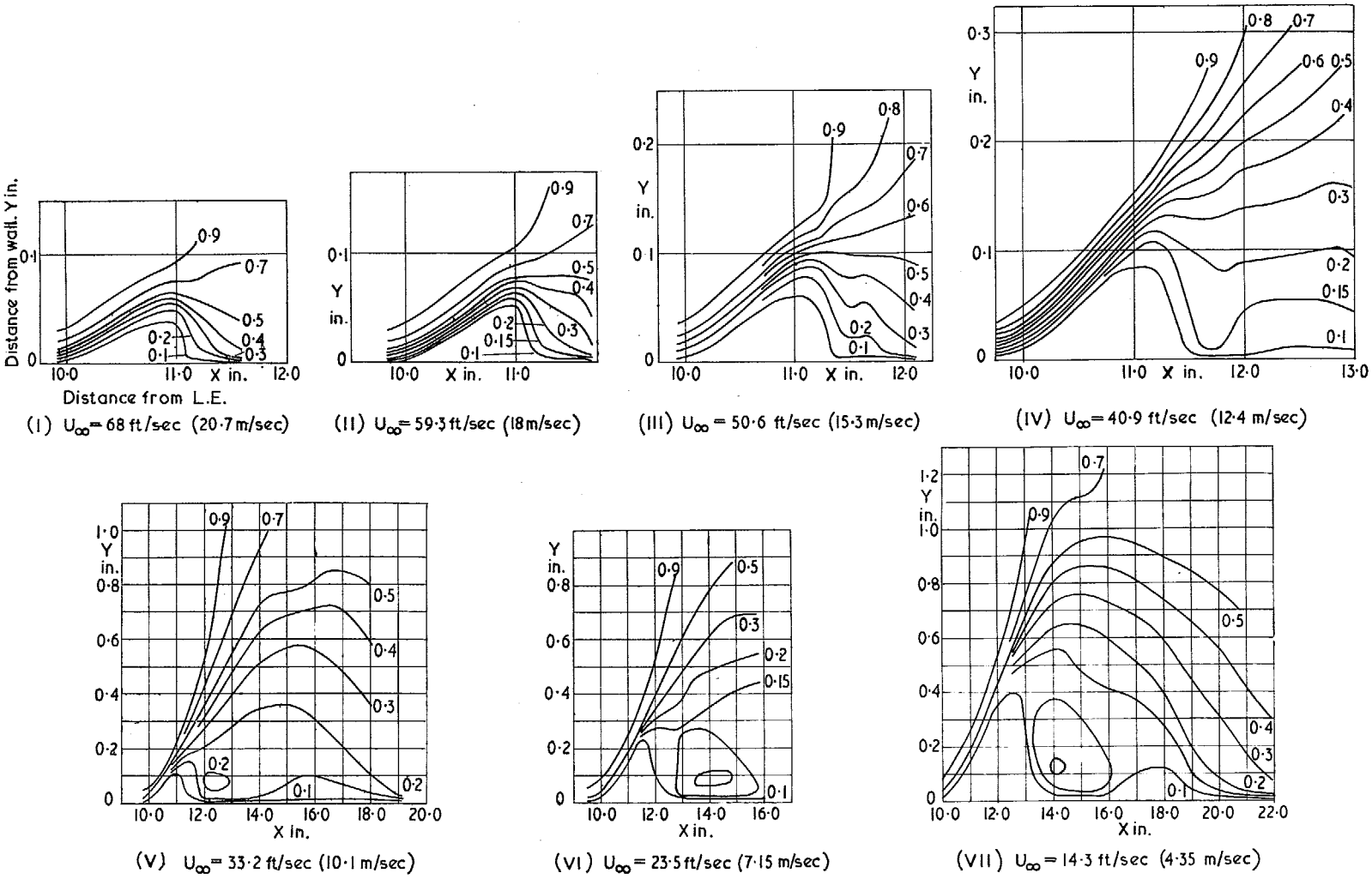

FIG. 8. Hot-wire velocity contours. Series II.

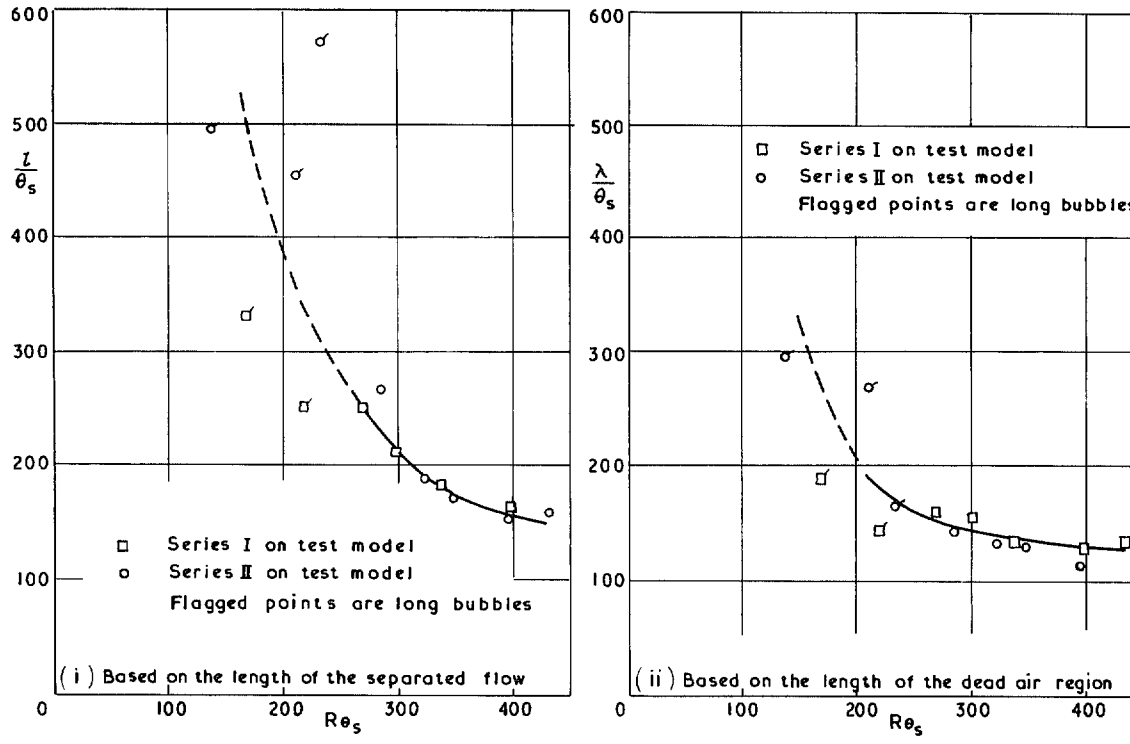

FIG. 9. Bubble length *versus* Reynolds number for Series I and II tests.

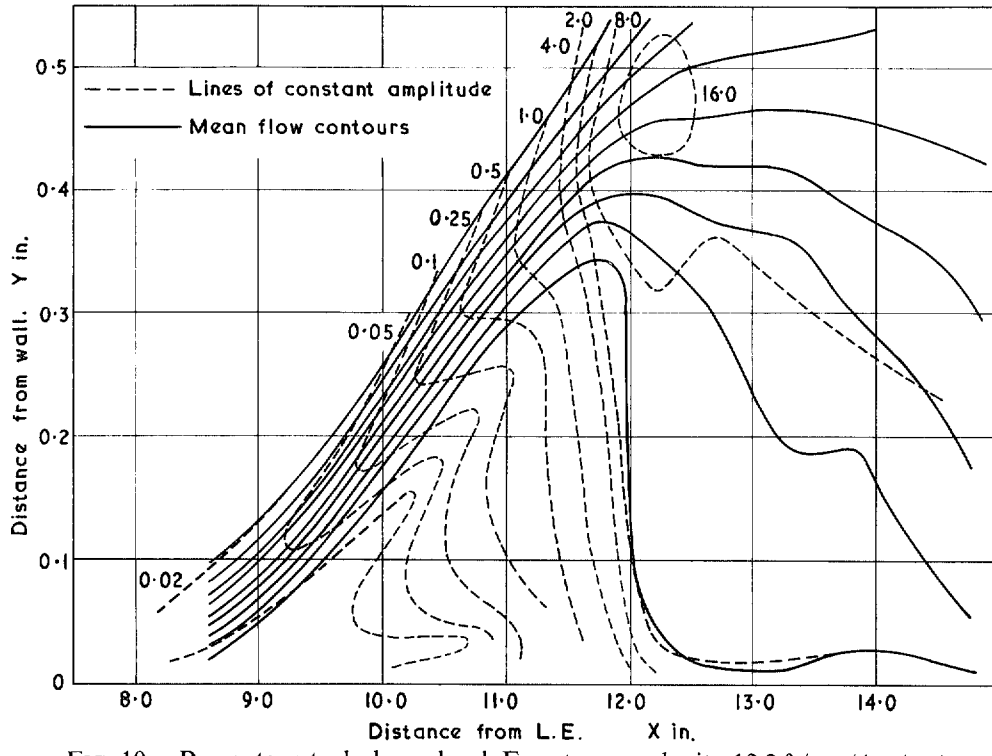

FIG. 10. Percentage turbulence level. Freestream velocity 13·2 ft/sec (4 m/sec).

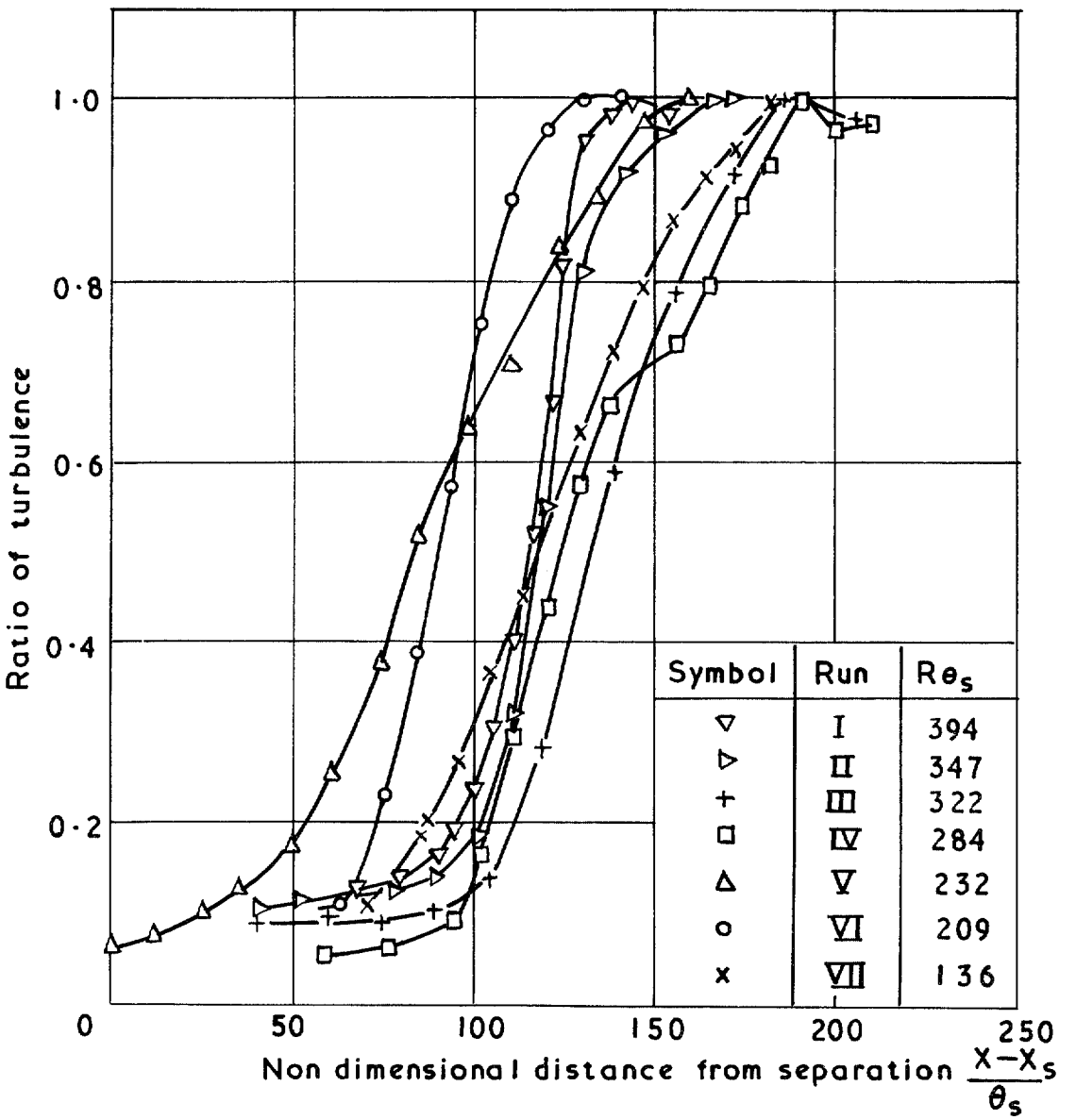

FIG. 11. Ratio of turbulence in the shear layer to the value at transition.

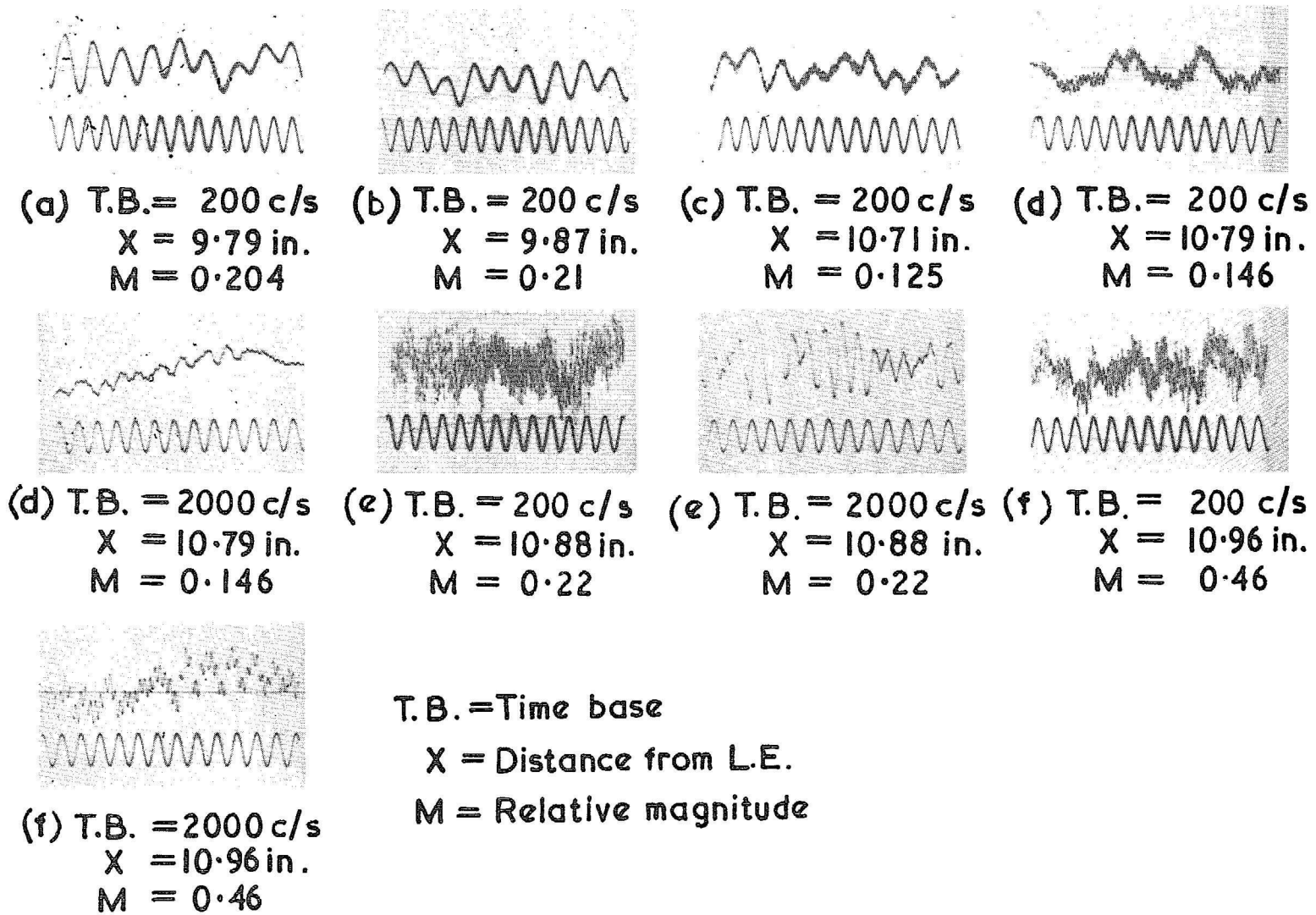

FIG. 12. Hot-wire signals in the centre of the shear layer Run (II).

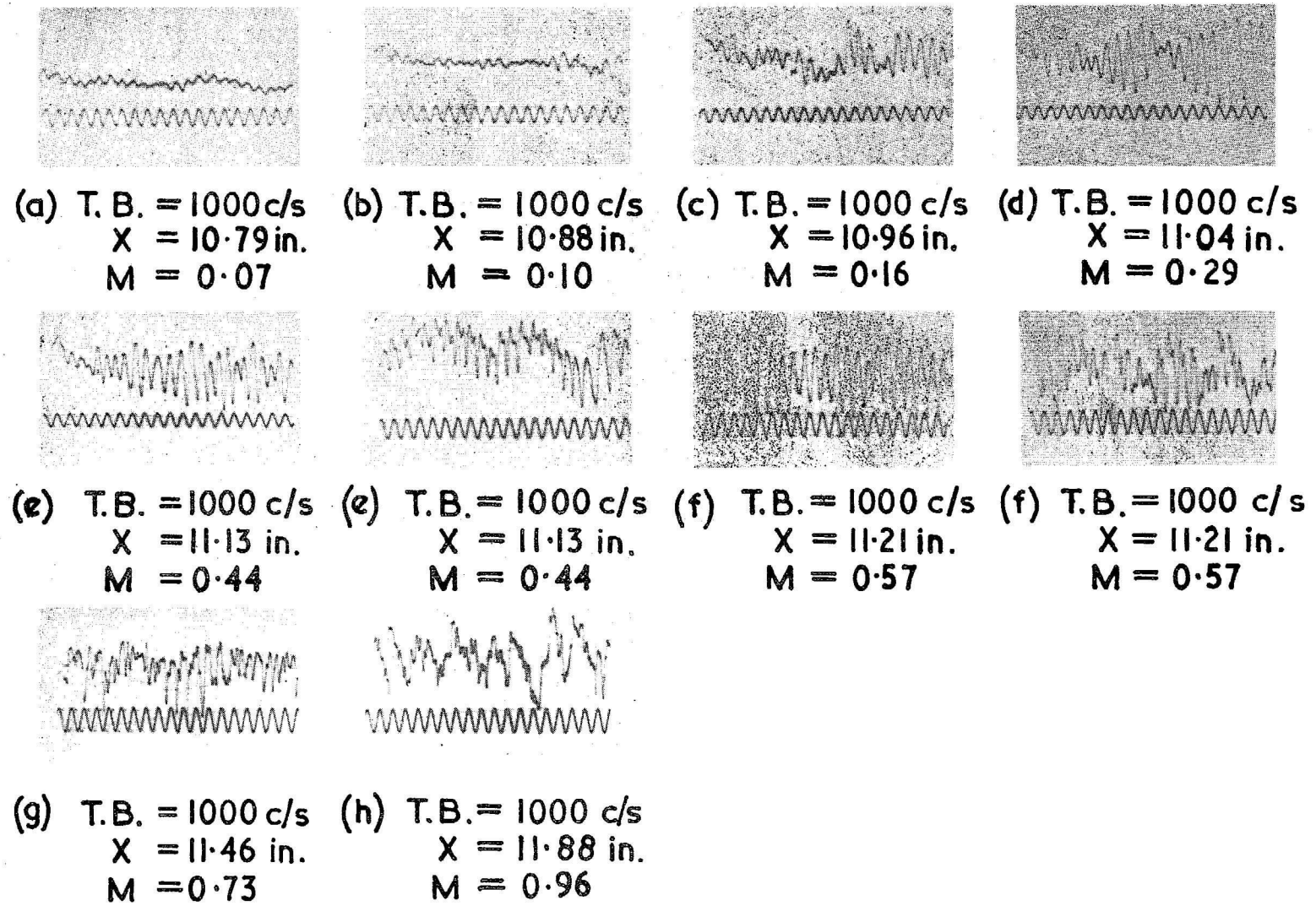

FIG. 13. Hot wire signals in the centre of the shear layer Run (IV).

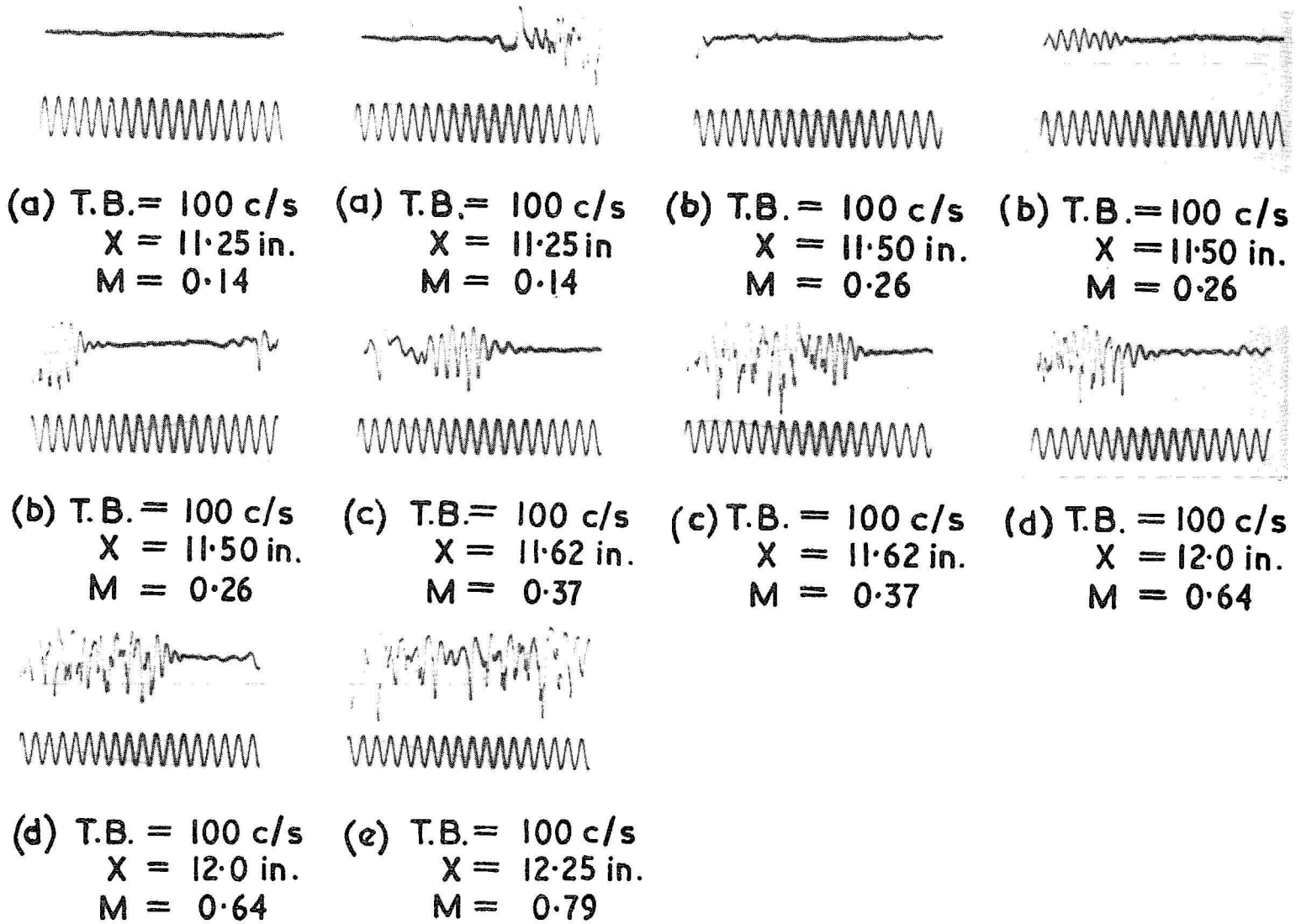

FIG. 14. Hot-wire signals in the centre of the shear layer Run VII.

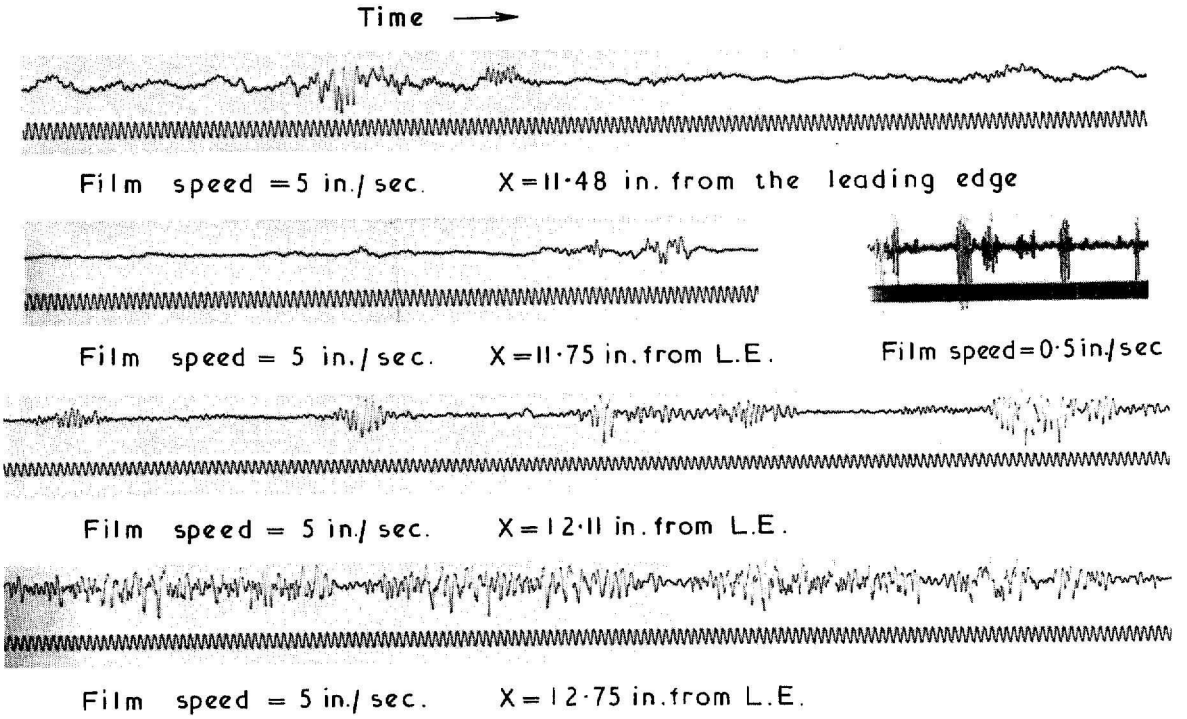

FIG. 15. Hot-wire records taken in a long bubble (VII). Time base = 100 c/s.

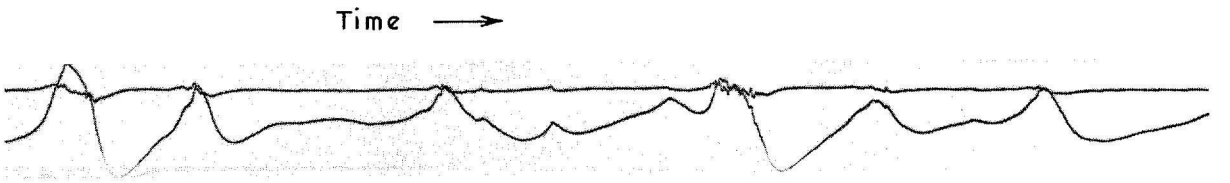

FIG. 16. Hot-wire recordings taken in a long bubble to demonstrate effect of low frequency oscillations on the creation of bursts. Film speed 2·5 in./sec. (Lower signal is the complete hot-wire output. Upper signal is the high frequency component.)

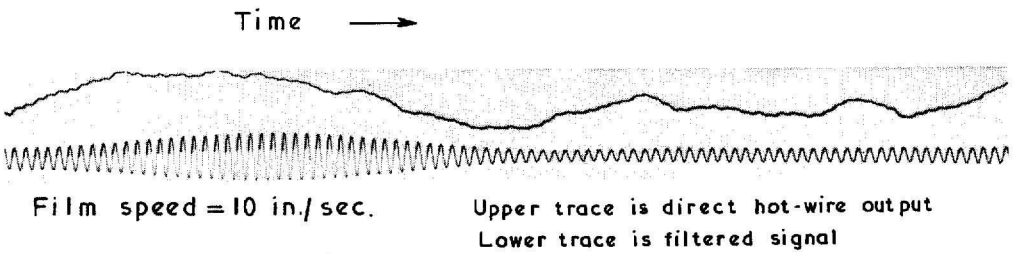

FIG. 17. Recordings of low and high frequency parts of the signal in a short bubble excited at 130 cycles/sec.

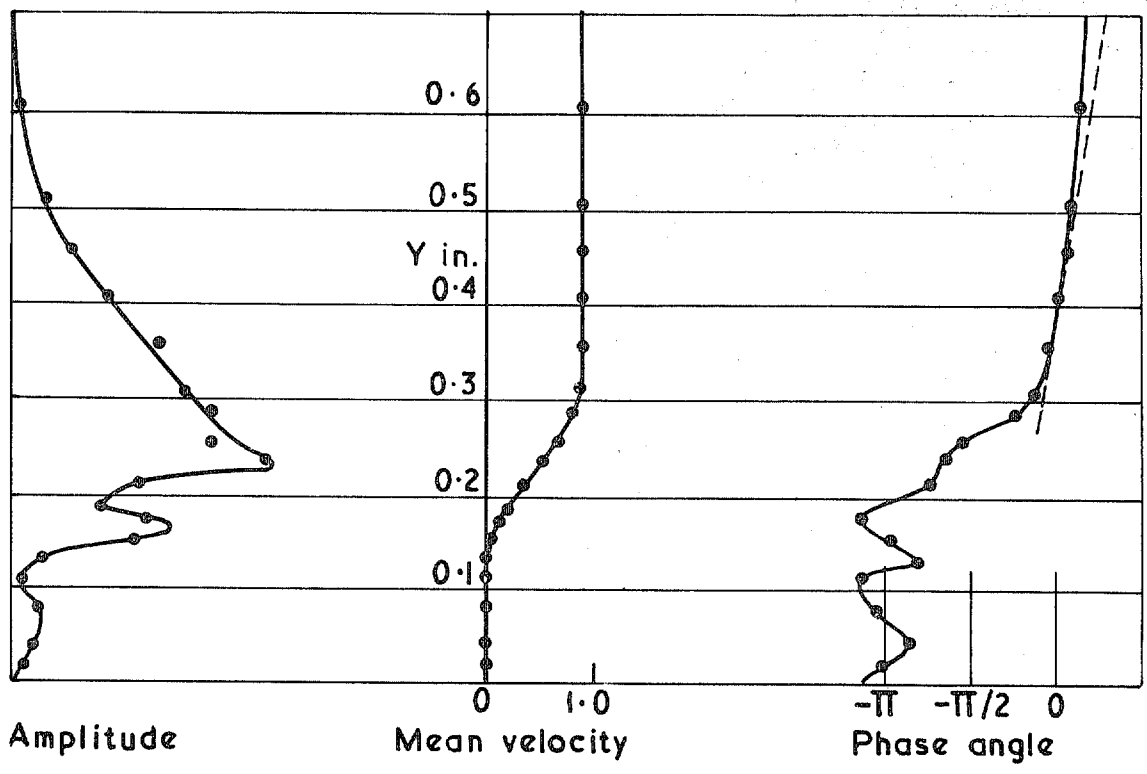

FIG. 18. Profile of bubble shown in Fig. 10 taken 11·4 in. from plate leading edge. Excitation 130 cycles per second.

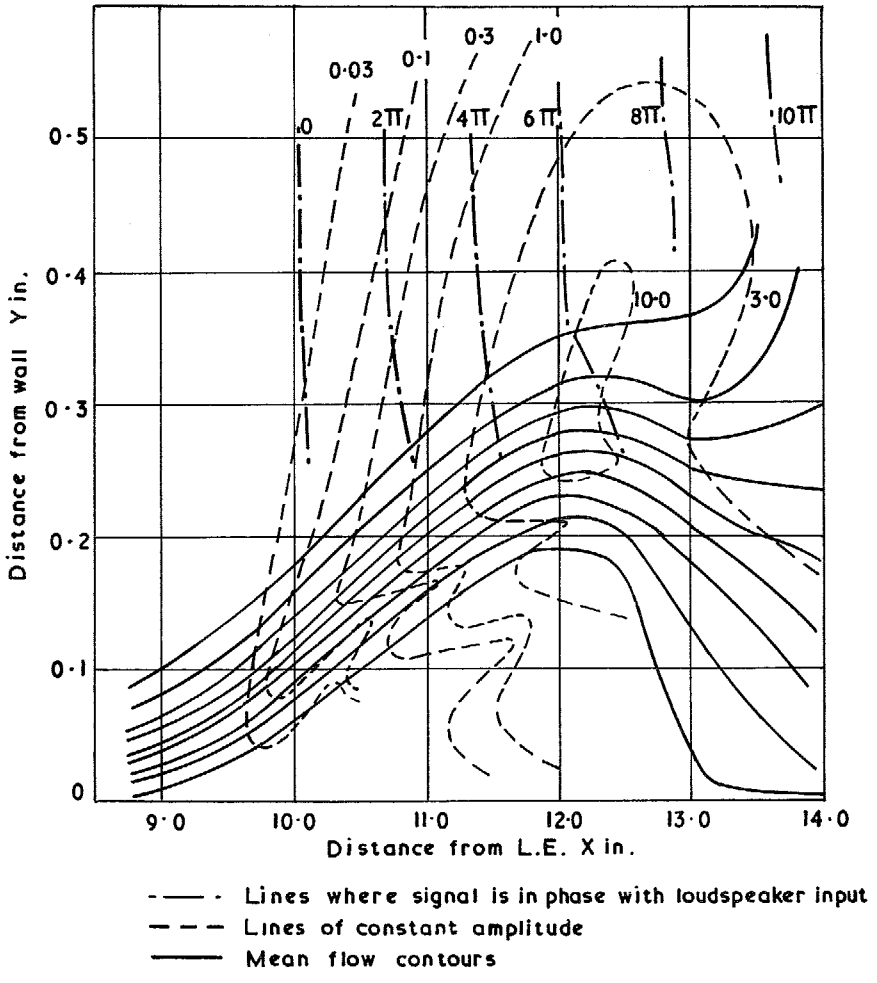

FIG. 19. Amplitude and phase constitution in wave excited by loudspeaker fed with 130 cycles/sec signal. Freestream velocity 13·2 ft/sec (4 m/sec).

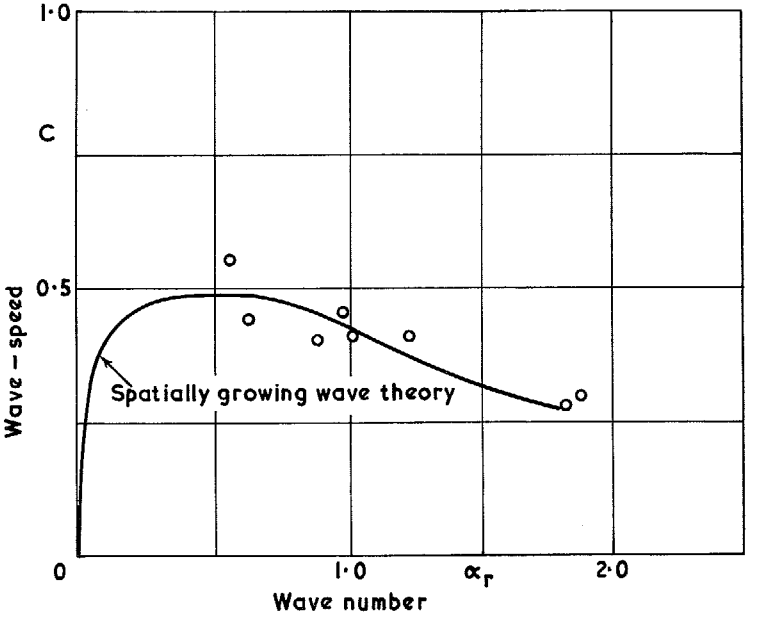

FIG. 20. Comparison of experimentally determined modes with those predicted from spatially growing theory.

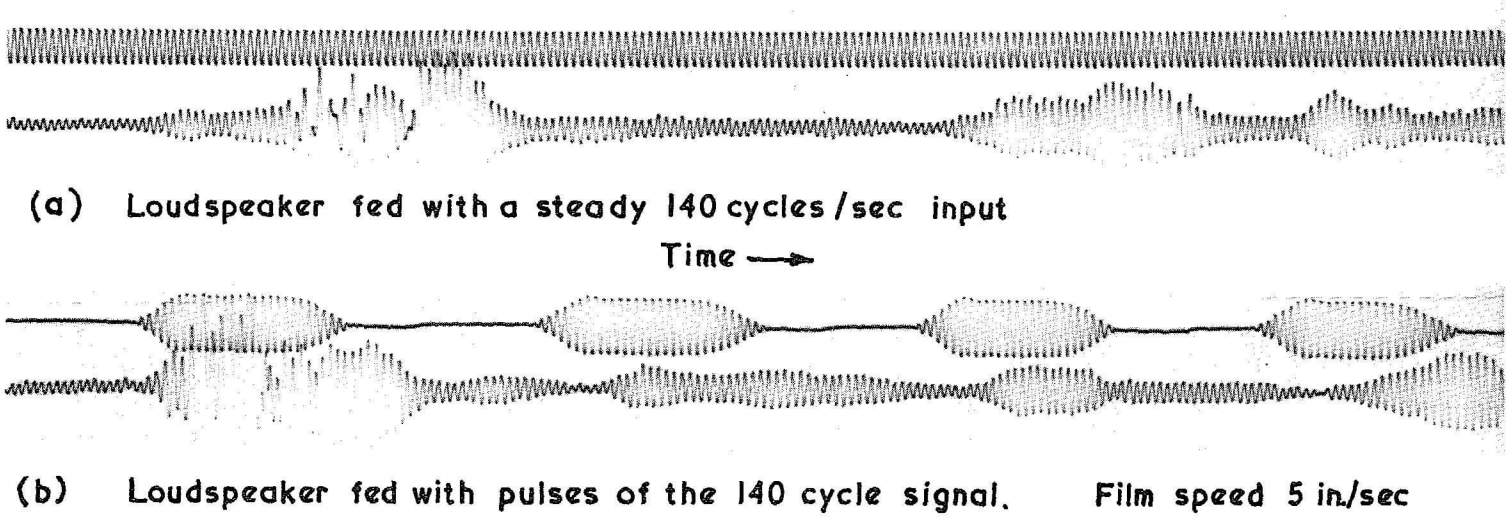

FIG. 21. Hot wire records taken in the long bubble (VII) at 11·75 in. from the leading edge excited by sound pulses.

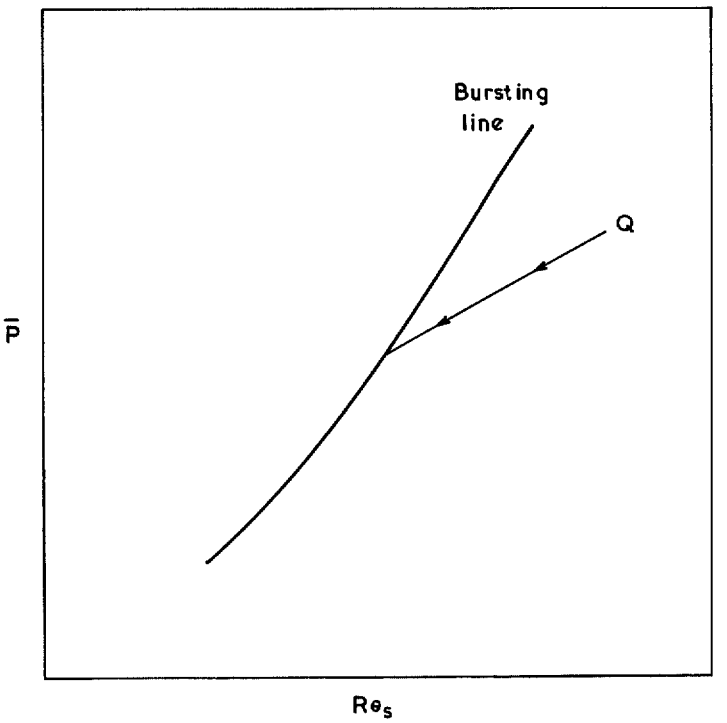

FIG. 22. Trajectory of a short bubble with falling speed.

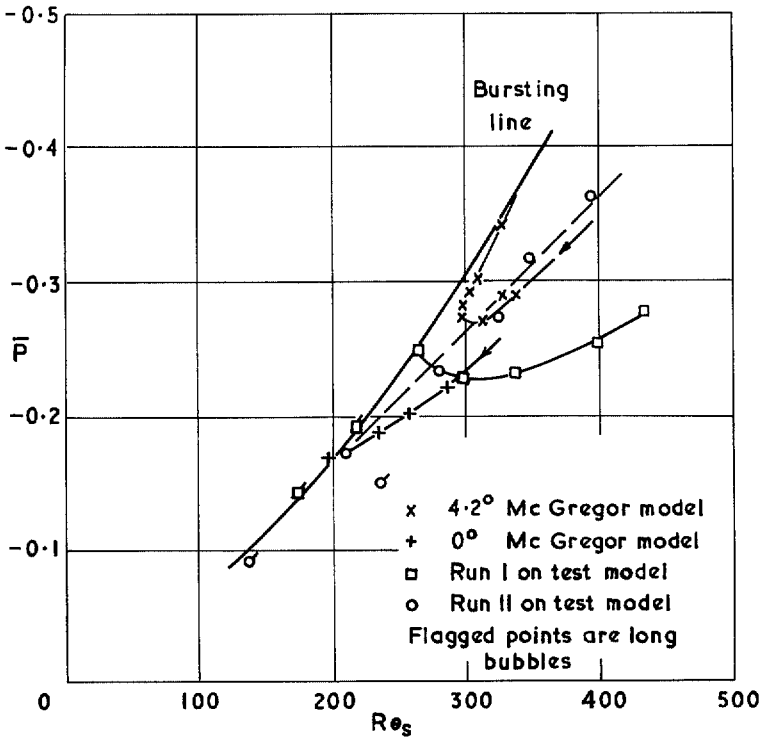

FIG. 23. The relationship between the pressure gradient parameter and Reynolds number with falling tunnel speed for various bubbles.

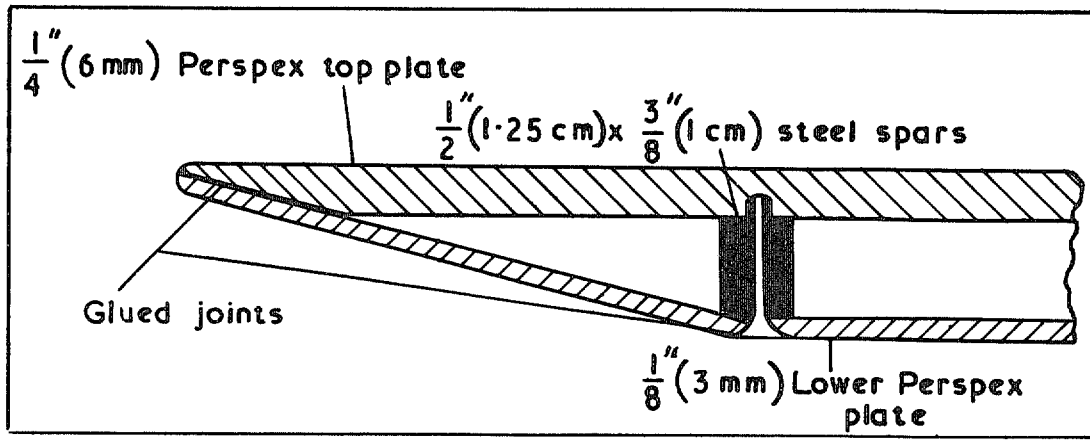

FIG. 24. Construction of plate leading edge.

Dd. 135646. K.5.

Printed in England for Her Majesty's Stationery Office by J. W. Arrowsmith Ltd., Bristol 3.

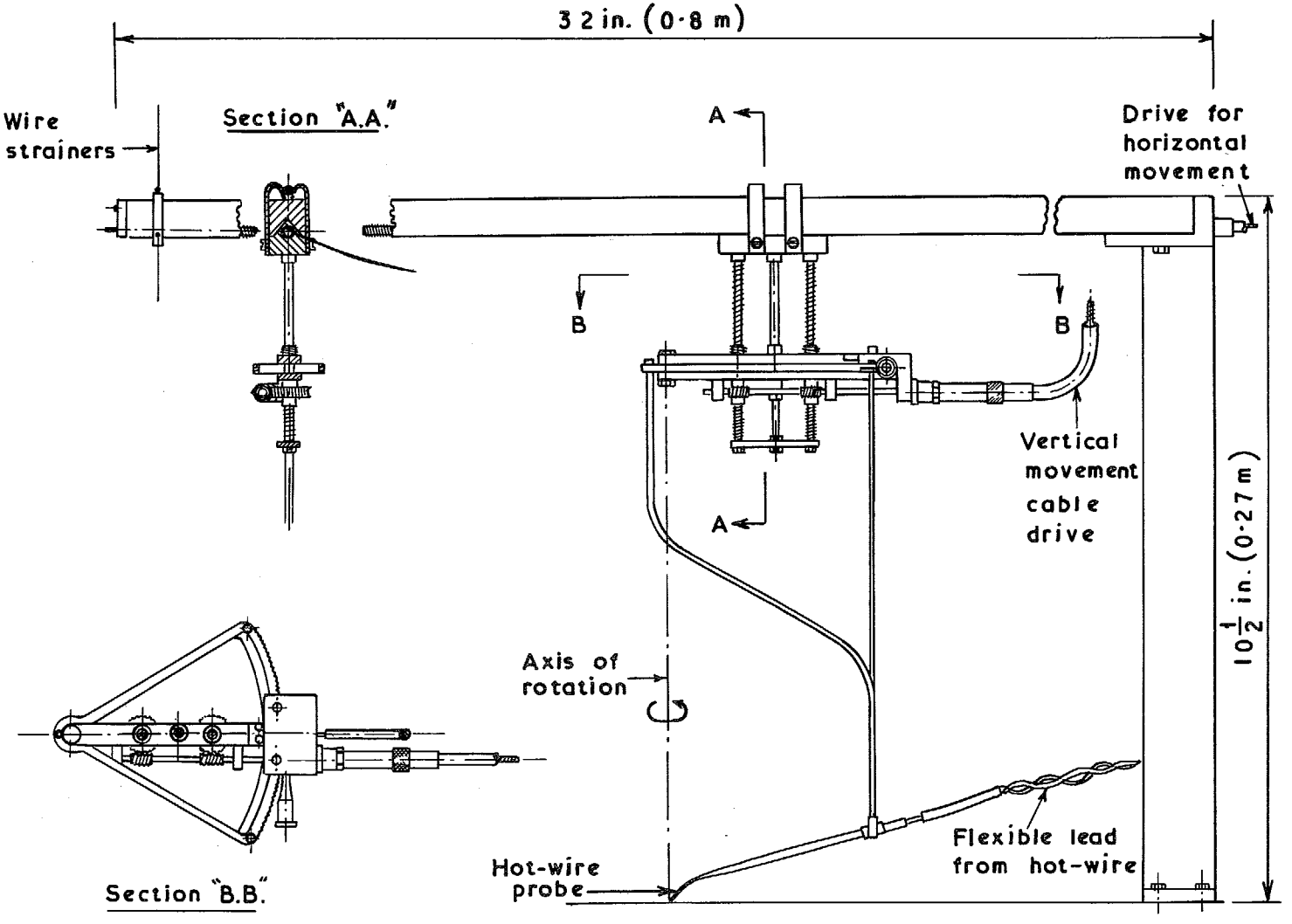

FIG. 25. Traversing apparatus.

Published by
HER MAJESTY'S STATIONERY OFFICE

To be purchased from
49 High Holborn, London W.C.1
13A Castle Street, Edinburgh EH2 3AR
109 St. Mary Street, Cardiff CF1 1JW
Brazennose Street, Manchester M60 8AS
50 Fairfax Street, Bristol BS1 3DE
258 Broad Street, Birmingham 1
7 Linenhall Street, Belfast BT2 8AY
or through any bookseller

R. & M. No. 3595

SBN 11 470192 X